JOURNAL OF GUIDANCE, CONTROL, AND DYNAMICS
Vol. 33, No. 1, January–February 2010

Modeling and Simulation of Hose-Paradrogue Aerial Refueling Systems

Kapseong Ro* and James W. Kamman*
Western Michigan University, Kalamazoo, Michigan 49008

DOI: 10.2514/1.45482

A dynamic modeling and simulation analysis of hose-paradrogue aerial refueling systems is presented. A set of governing equations of motion is derived using a finite-segment approach that describes the dynamics of the hose-paradrogue assembly under a prescribed motion of the tanker. The hose is modeled by a series of ball-and-socket-connected rigid links subject to gravitational and aerodynamic loads that account for the effects of tanker wake, steady wind, and atmospheric turbulence. Numerical simulations show a good correlation of the model's steady-state characteristics with previously reported flight-test data. Also investigated are the dynamic characteristics of the paradrogue assembly resulting from atmospheric turbulence and a typical pitch doublet maneuver of the tanker. Finally, the dynamic motion resulting from an in-flight adjustment of the paradrogue drag associated with strut-angle changes is studied.

Nomenclature

$\boldsymbol{a}_K$	=	acceleration of lumped mass K, ft/s^2
$\boldsymbol{a}_0$	=	acceleration of the system tow point (hose exit point from a pod), ft/s^2
B^*	=	vehicle mass center
C_{drogue}	=	drag coefficient of paradrogue
$C_{X_N Z_N}$	=	vertical plane in which the aircraft moves
$c_{n,K}$, $c_{t,K}$	=	normal and tangential drag coefficient of the link K
$\boldsymbol{D}_K$	=	aerodynamic force acting on link K, lb
d_K, d_{drogue}	=	diameters of link K and paradrogue
F_K	=	frame fixed in link K with axes (x_K, y_K, z_K)
F_N	=	inertial frame with axes (X_N, Y_N, Z_N)
F_W	=	aircraft (tanker) mean air trajectory frame with axes (X_W, Y_W, Z_W)
$\widehat{GS}$	=	normalized paradrogue gore spacing; ranges from $(-1$–$1)$ for gore spacing from 5–8.5 deg
$\boldsymbol{g}$	=	gravitational acceleration vector, ft/s^2
L_H	=	straight-line distance from hose exit point to paradrogue coupling, ft
ℓ_K	=	length of link K, ft
m_{drogue}	=	mass of paradrogue, slug
m_K	=	mass of lumped mass K (one-half of the total mass of adjoining links), slug
N	=	number of links
$\boldsymbol{n}_{K1}$, $\boldsymbol{n}_{K2}$, $\boldsymbol{n}_{K3}$	=	mutually perpendicular unit vectors fixed in link K
$\boldsymbol{n}_{K1}$	=	unit vector pointing from lumped mass K to lumped mass J (along link K
O_N	=	origin of the inertial frame
$\boldsymbol{p}_K$	=	position vector of lumped mass K relative to J; components in F_W, ft
$\boldsymbol{p}_{K,\theta_{Ki}}$	=	$\partial \boldsymbol{p}_K / \partial \theta_{Ki}$, ft
$\boldsymbol{Q}_K$	=	external force vector acting on lumped mass K (one-half of the total force acting on the adjoining links), lb
$\boldsymbol{r}_K$	=	position vector of lumped mass K relative to an inertial frame, ft
$\widehat{SA}$	=	normalized paradrogue canopy characteristic length, ranges from $(-1$–$1)$ for lengths from 3–5.5 in. (7.62–13.97 cm)
S_{Ki}, C_{Ki}	=	sine and cosine of θ_{Ki}
t_K	=	tension in link K, lb
$\boldsymbol{u}_K$	=	local air velocity due to steady wind, tanker wake, and turbulence at lumped mass K, ft/s
V_D	=	altitude difference from hose exit point to paradrogue coupling, ft
V_∞	=	tanker speed, ft/s
$\boldsymbol{v}_{B^*}(t)$	=	inertial velocity of the vehicle mass center, ft/s
$\boldsymbol{v}_K$	=	velocity of lumped mass K, ft/s
$\boldsymbol{v}_{K/\text{air}}$	=	velocity of lumped mass K relative to the local air velocity $(\boldsymbol{v}_K - \boldsymbol{u}_K)$, ft/s
$\boldsymbol{v}_{K,n}$, $\boldsymbol{v}_{K,t}$	=	vector components of $\boldsymbol{v}_K$ normal and tangent to link K, ft/s
$\boldsymbol{w}_1$, $\boldsymbol{w}_2$, $\boldsymbol{w}_3$	=	mutually perpendicular unit vectors fixed in F_W
$\hat{\alpha}$	=	normalized strut angle of paradrogue; ranges from $(-1$–$1)$ for strut angles from 45–90 deg
$\boldsymbol{\alpha}_W$	=	angular acceleration of the frame F_W relative to F_N, rad/s^2
$\gamma(t)$	=	aircraft flight-path (trajectory) angle, deg
θ_{K1}, θ_{K2}	=	orientation angles of link K defining its orientation relative to F_W, deg
μ_K	=	reciprocal of mass m_K, $1/m_K$, 1/slug
ρ_∞	=	local freestream air density, slug/ft^3
$\boldsymbol{\omega}_W$	=	angular velocity of frame relative to F_N, rad/s

I. Introduction

AS WITNESSED in numerous military operations over the past two decades, the number of unmanned aerial vehicles (UAVs) is growing rapidly. Given this trend, it is likely they will dominate the future airspace. Increasing demands in UAV technology require not only a larger number of UAVs to be manufactured and deployed but also extensive research and development for innovative technological breakthroughs. One of the challenging issues for future UAV operations is associated with coordinated operations of a UAV with other vehicles in close proximity. This occurs during operations such as aerial refueling, aerial recovery, formation flying, and swarming.

Automated aerial refueling (AAR) procedures have been under substantial investigation in recent years, and several technical challenges have been identified [2,3]. Two types of aerial refueling methods are practiced: one uses a hose-paradrogue-probe assembly

Presented as Paper 1849 at the AIAA Infotech@Aerospace Conference, Seattle, WA, 6–9 April 2009; received 15 May 2009; revision received 16 September 2009; accepted for publication 22 September 2009.

*Associate Professor, Department of Mechanical and Aeronautical Engineering. Member AIAA.

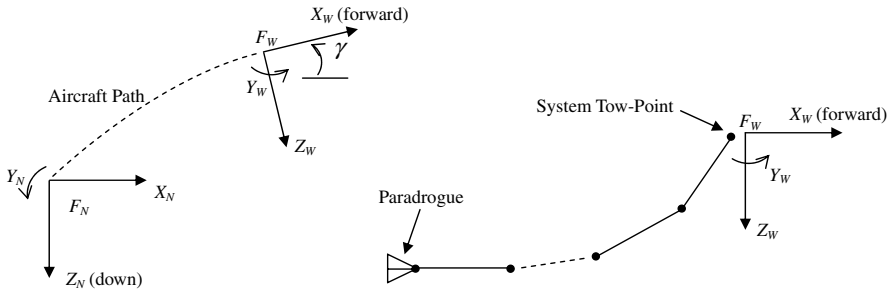

Fig. 1 Side views of the reference frames and the hose-drogue system.

and the other uses a boom-receptacle system. At this time, there is considerable interest in both methods [4].

Based on cost and operational considerations, the hose-paradrogue-probe-based refueling method is appealing for UAV operations, especially with recent and continued improvement of UAV automatic control strategies. However, even though some progress has been made to automate the refueling process using vision-based control and navigation techniques [5], skillful piloting of the receiver aircraft is still essential.

The objective of the current study is to develop a system dynamic model that accurately captures the motion of a hose-paradrogue assembly under prescribed motion of the tanker aircraft. Such a model can be used to carry out various model-based design studies including an AAR procedure.

The mathematical and numerical methods required to model the dynamics of laterally flexible structures (such as cables) have been developed for many applications over the last 30–50 years, and thus the related literature is very rich and accessible in the public domain. However, only a limited number of papers can be found that apply these methods specifically to the hose-paradrogue aerial refueling problem. Zhu and Meguid [6] presented a good literature review for aerial towed system analysis, and they proposed a new locking-free, curved-beam, finite element formulation that overcomes the difficulties of classical cable theory in treating large rotations and deformations of the refueling assembly. Apart from the aerospace community, modeling of submerged cable dynamics has also been of interest for the past several decades in the marine engineering community [7]. One of these modeling methods is a lumped-mass, finite-segment approach in which a cable is modeled by a series of rigid links connected with ball-and-socket joints [8]. Each link is subject to gravitational and fluid dynamic loads. The link masses and all external forces are lumped at the connecting joints.

In this paper, a governing system dynamic model of an aerial refueling hose-paradrogue assembly is developed using the finite-segment approach. The model describes the dynamic motion of the hose-paradrogue assembly in the wake of a tanker executing a predetermined trajectory. A MATLAB® script-based computer program was developed for numerical simulation studies, and the results are compared to those flight-test results and simulation results available in the open literature [2,3,9–12]. An adjustable-drag paradrogue-assembly aerodynamic model [1] is used to study the possibility of stabilizing and steering its position over a broad speed range.

II. Formulation of Equations of Motion

The hose-paradrogue assembly is modeled as a link-connected system, where the hose consists of a finite number of cylindrically shaped rigid links connected with frictionless spherical joints. The masses and loads associated with each link are concentrated at the joints. The paradrogue is treated as a lumped mass at the end of the hose. Its drag may be considered adjustable in flight. The other end of the assembly is connected to a refueling pod (towing point) for which the motion is specified relative to the aircraft (tanker) mean trajectory frame. The assembly is subject to gravitational and aerodynamic loads that account for the tanker wake, steady wind, and atmospheric turbulence.

A. Kinematics

1. Reference Frames and System Configuration

Figure 1 depicts the hose-paradrogue-assembly model. F_N represents an inertial reference frame in which the system moves, and F_W represents the mean trajectory frame of the tanker. Here, X_W is pointed forward along the trajectory, Y_W is normal to the trajectory plane, and Z_W is directed to make F_W a right-handed coordinate system. Initially, the aircraft mean trajectory axes (X_W, Y_W, Z_W) are assumed to be aligned with the inertial frame axes (X_N, Y_N, Z_N). Then the origin of F_W (typically the aircraft mass center B^*) moves in the vertical plane $C_{X_N Z_N}$ in accordance with a prescribed aircraft velocity $\boldsymbol{v}_{B^*}(t)$ and the trajectory (or flight-path) angle $\gamma(t)$.

The motion of the system tow point (hose exit point) and the orientations of the hose links are all defined relative to the aircraft mean trajectory frame F_W. The tow point can have motion relative to F_W in each of the X_W, Y_W, and Z_W directions to account for aircraft motion (such as motion due to atmospheric turbulence) relative to the aircraft mean trajectory. The orientations of the hose links are described relative to F_W using body-fixed rotation sequences. To orient a hose link relative to F_W, first align it with the $-X_W$ axis and define a set of link-fixed axes x_K, y_K, and z_K parallel to the X_W, Y_W, and Z_W directions. Then rotate the link downward about the Y_W (or y_K) axis and outward about the link-fixed z_K axis. Using this approach, only

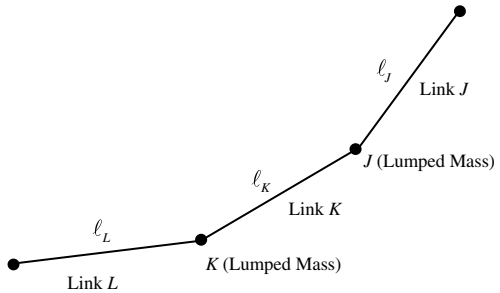

Fig. 2 Typical links and lumped masses.

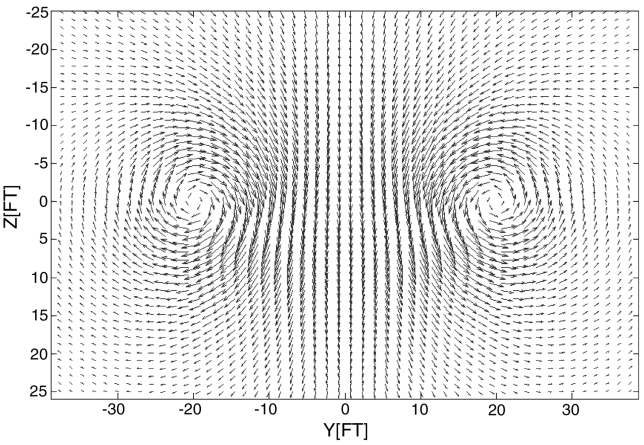

Fig. 3 Vertical slice of tanker wake (50 ft aft) ($V_\infty = 210$ kt and alt = 7500 ft).

the first link angle will be nonzero for motion of the system in $C_{X_N Z_N}$. The paradrogue is not treated as a separate body; its weight and drag are added to the lumped mass at the end of the hose.

2. System Motion

Given the motion of the frame F_W, the motion of the system tow point relative to F_W, and the link angles and their derivatives, the motion of any point in the system may be found. Consider, for example, a typical link K with associated lumped masses J and K, as shown in Fig. 2. The lumped mass J is at the upper end of the link (closer to the aircraft). The position vector of lumped mass K relative to the origin O_N of the inertial frame may then be expressed as

$$\boldsymbol{r}_K = \boldsymbol{r}_J + \boldsymbol{p}_K \tag{1}$$

Using the link-fixed rotation sequence described above, $\boldsymbol{p}_K$ may be written as

$$\boldsymbol{p}_K = -\ell_K(C_{K1}C_{K2}\boldsymbol{w}_1 + S_{K2}\boldsymbol{w}_2 - S_{K1}C_{K2}\boldsymbol{w}_3 \tag{2}$$

Along with the motion of F_W and the system tow point, Eqs. (1) and (2) may be used recursively to find the positions of all lumped masses. Recursive relations for the velocities and accelerations of the lumped masses may be found by differentiating in the inertial frame F_N:

$$\boldsymbol{v}_K = \boldsymbol{v}_J + \dot{\boldsymbol{p}}_K \qquad \boldsymbol{a}_K = \boldsymbol{a}_J + \ddot{\boldsymbol{p}}_K \tag{3}$$

The derivatives of $\boldsymbol{p}_K$ may be expressed as

$$\dot{\boldsymbol{p}}_K = \sum_i (\boldsymbol{p}_{K,\theta_{Ki}}\dot{\theta}_{Ki}) + (\boldsymbol{\omega}_W \times \boldsymbol{p}_K) \tag{4}$$

$$\ddot{\boldsymbol{p}}_K = \sum_i (\boldsymbol{p}_{K,\theta_{Ki}}\ddot{\theta}_{Ki}) + \sum_i (\dot{\boldsymbol{p}}_{K,\theta_{Ki}}\dot{\theta}_{Ki}) + (\boldsymbol{\alpha}_W \times \boldsymbol{p}_K) + \boldsymbol{\omega}_W \times \dot{\boldsymbol{p}}_K) \tag{5}$$

Taking the scalar product of Eq. (5) with $\boldsymbol{p}_{K,\theta_{Ki}}$ and noting that $\boldsymbol{p}_{K,\theta_{K1}} \cdot \boldsymbol{p}_{K,\theta_{K2}}$ is zero, the second derivative of the angles for any link may be expressed as

$$\ddot{\theta}_{Kj} = \boldsymbol{p}_{K,\theta_{Kj}} \cdot \left[\boldsymbol{a}_K - \boldsymbol{a}_J - \sum_i (\dot{\boldsymbol{p}}_{K,\theta_{Ki}}\dot{\theta}_{Ki}) - (\boldsymbol{\alpha}_W \times \boldsymbol{p}_K) - (\boldsymbol{\omega}_W \times \dot{\boldsymbol{p}}_K)\right] \Big/ (\boldsymbol{p}_{K,\theta_{Kj}} \cdot \boldsymbol{p}_{K,\theta_{Kj}}) \qquad (j = 1, 2) \tag{6}$$

Given the accelerations of the lumped masses, the link orientation angles and their time derivatives, and the angular motion of frame F_W, the second derivatives of all link angles may be individually calculated.

Table 1 Physical characteristics of the tanker and hose-paradrogue assembly

Component	Configuration
Tanker (F/A-18A)	
Weight, lb	45,310
Span, ft	37.5
Reference area, ft^2	400
Hose	
Length, ft	47.0
Diameter (internal), in.	2.00
Diameter (external), in.	2.65
Weight/Length, lb/ft	2.75
Drogue	
Weight, lb	65
Diameter, ft^2	2.0

B. Equations of Motion

1. Lumped Masses

Applying Newton's laws to a typical lumped mass K along the hose gives

$$\boldsymbol{a}_K = (\boldsymbol{Q}_K + \boldsymbol{t}_K + \boldsymbol{t}_L)/m_K = \mu_K(\boldsymbol{Q}_K + \boldsymbol{t}_K + \boldsymbol{t}_L) \tag{7}$$

These equations alone cannot be used to compute the motion of the system. They must be augmented with a set of constraint equations to ensure rigidity of the connecting links.

2. Hose Tensions

Assuming the hose links all have constant length, the accelerations of adjacent lumped masses may be related as follows. First write $(\boldsymbol{p}_K \cdot \boldsymbol{p}_K) = \ell_K^2$, and then differentiate twice to get

$$(\boldsymbol{a}_K - \boldsymbol{a}_J) \cdot \boldsymbol{n}_{K1} = \ell_K \dot{\boldsymbol{n}}_{K1}^2 \tag{8}$$

Substituting accelerations from Eq. (7) into Eq. (8) gives a set of linear algebraic equations for the link tensions

Table 2 Computed steady-state characteristics of hose-paradrogue assembly ($C_{\text{drogue}} = 0.8$)

	Altitude, ft			
Steady-state values	7500	10,000	25,000	30,000
	Speed of 170 kt			
D_{drogue}, lb	211.57	197.61	132.46	117.10
$T_{\max}$, lb	269.74	258.29	210.08	201.01
L_H, ft	46.92	46.92	46.94	46.95
V_D, ft	21.45	22.48	29.31	31.82
DDVP	0.46	0.48	0.62	0.68
	Speed of 190 kt			
D_{drogue}, lb	258.71	240.91	156.91	136.65
$T_{\max}$, lb	310.11	294.61	226.84	212.78
L_H, ft	46.92	46.92	46.93	46.93
V_D, ft	18.62	19.59	26.23	28.73
DDVP	0.40	0.42	0.56	0.61
	Speed of 210 kt			
D_{drogue}, lb	311.83	289.83	185.13	159.50
$T_{\max}$, lb	357.71	337.79	248.31	228.72
L_H, ft	46.93	46.93	46.92	46.93
V_D, ft	16.25	17.15	23.50	25.94
DDVP	0.35	0.37	0.50	0.55
	Speed of 230 kt			
D_{drogue}, lb	370.79	344.20	216.93	185.41
$T_{\max}$, lb	412.20	387.45	274.24	248.52
L_H, ft	46.94	46.93	46.92	46.92
V_D, ft	14.25	15.09	21.09	23.47
DDVP	0.30	0.32	0.45	0.50
	Speed of 250 kt			
D_{drogue}, lb	435.48	403.91	252.26	214.42
$T_{\max}$, lb	473.31	443.34	304.47	272.15
L_H, ft	46.95	46.94	46.92	46.92
V_D, ft	12.57	13.34	18.96	21.27
DDVP	0.27	0.28	0.40	0.45
	Speed of 270 kt			
D_{drogue}, lb	505.84	468.88	290.96	246.35
$T_{\max}$, lb	540.82	505.25	338.79	299.32
L_H, ft	46.95	46.95	46.93	46.92
V_D, ft	11.14	11.85	17.10	19.28
DDVP	0.24	0.25	0.36	0.41
	Speed of 290 kt			
D_{drogue}, lb	581.83	539.09	332.96	281.08
$T_{\max}$, lb	614.59	573.00	377.08	329.92
L_H, ft	46.96	46.96	46.93	46.93
V_D, ft	9.92	10.57	15.47	17.54
DDVP	0.21	0.23	0.33	0.37
	Speed of 310 kt			
D_{drogue}, lb	663.40	614.47	378.21	318.58
$T_{\max}$, lb	694.45	646.47	419.16	363.90
L_H, ft	46.97	46.96	46.94	46.93
V_D, ft	8.88	9.48	14.04	16.00
DDVP	0.19	0.20	0.30	0.34

$$-\mu_J(\boldsymbol{n}_{J1}\cdot\boldsymbol{n}_{K1})t_J+(\mu_J+\mu_K)t_K-\mu_K(\boldsymbol{n}_{L1}\cdot\boldsymbol{n}_{K1})t_L = \ell_K\dot{\boldsymbol{n}}_{K1}^2+(\mu_J\boldsymbol{Q}_J-\mu_K\boldsymbol{Q}_K).\boldsymbol{n}_{K1} \tag{9}$$

or, in matrix form,

$$[T]\{t\}=\{q\} \tag{10}$$

Here, the coefficient matrix $[T]$ is tridiagonal. The entries of $[T]$ for rows other than the first and last, and the entries of $\{q\}$ for rows other than the first may be read directly from Eq. (9). The remaining entries are as follows.

For row $K=1$ and $L=2$,

$$T_{11}=\mu_K \qquad T_{12}=-\mu_K(\boldsymbol{n}_{L1}\cdot\boldsymbol{n}_{K1}) \tag{11}$$

For row $K=N-1$ and $K=N$,

$$T_{K,(K-1)}=-\mu_J(\boldsymbol{n}_{J1}\cdot\boldsymbol{n}_{K1}) \qquad T_{KK}=\mu_J+\mu_K \tag{12}$$

For row $K=1$,

$$q_1=\ell_K\dot{\boldsymbol{n}}_{K1}^2-\mu_K(\boldsymbol{Q}_K\cdot\boldsymbol{n}_{K1})+(\boldsymbol{a}_0\cdot\boldsymbol{n}_{K1}) \tag{13}$$

C. External Forces

1. Forces on Lumped Mass

The resultant external force $\boldsymbol{Q}_K$ acting on the lumped mass K, including both gravitational and aerodynamic forces, is

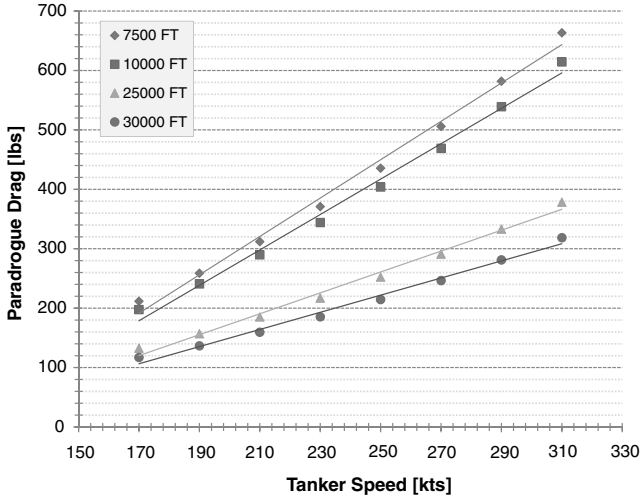

Fig. 4 Steady-state drag of paradrogue from Table 2.

$$\boldsymbol{Q}_K=m_K\boldsymbol{g}+\tfrac{1}{2}(\boldsymbol{D}_{K-1}+\boldsymbol{D}_K) \tag{14}$$

where $\boldsymbol{D}_K$ may be computed as

$$\boldsymbol{D}_K=\left\{-\frac{1}{2}\rho_\infty[\boldsymbol{v}_{K/\text{air}}\cdot\boldsymbol{n}_{K1}]^2(\pi d_K\ell_K)c_{t,K}\right\}\boldsymbol{n}_{K1} +\left\{-\frac{1}{2}\rho_\infty\|\boldsymbol{v}_{K/\text{air}}-(\boldsymbol{v}_{K/\text{air}}\cdot\boldsymbol{n}_{K1})\boldsymbol{n}_{K1}\|^2(d_K\ell_K)c_{n,K}\right\} \times\frac{[\boldsymbol{v}_{K/\text{air}}-(\boldsymbol{v}_{K/\text{air}}\cdot\boldsymbol{n}_{K1})\boldsymbol{n}_{K1}]}{\|\boldsymbol{v}_{K/\text{air}}-(\boldsymbol{v}_{K/\text{air}}\cdot\boldsymbol{n}_{K1})\boldsymbol{n}_{K1}\|} \tag{15}$$

The normal and tangential drag coefficients are dependent upon the Reynolds number of the local flow and may be obtained from experimental sources [10,13]. The local air velocity $\boldsymbol{u}_K$ is due to the wake of the tanker, steady wind, and atmospheric turbulence. The air velocity due to the tanker wake can be modeled using a Helmholtz horseshoe-vortex model [14,15]. The model contains velocity components in all three spatial directions. Figure 3 illustrates a typical vertical slice of the wake 50 ft behind the aircraft for an altitude of 7500 ft (2286 m) and airspeed of 210 kt (354 ft/s or 108 m/s).

At the end of the hose where the paradrogue is connected, the resultant external force is

$$\boldsymbol{Q}_N=(m_N+m_{\text{drogue}})\boldsymbol{g}+\tfrac{1}{2}\boldsymbol{D}_N+\boldsymbol{D}_{\text{drogue}} \tag{16}$$

2. Drag of Paradrogue Assembly

The drag of the paradrogue assembly can be computed as

$$\boldsymbol{D}_{\text{drogue}}=-\frac{1}{2}\rho_\infty(\boldsymbol{v}_{N/\text{air}}\cdot\boldsymbol{v}_{N/\text{air}})\left(\frac{\pi d_{\text{drogue}}^2}{4}\right)C_{\text{drogue}}\left(\frac{\boldsymbol{v}_{N/\text{air}}}{\|\boldsymbol{v}_{N/\text{air}}\|}\right) \tag{17}$$

The drag coefficient C_{drogue} depends on the paradrogue's geometric characteristics. Reference [1] used wind-tunnel data to develop an empirical formula for C_{drogue} as a function of a set of normalized geometric characteristics:

$$C_{\text{drogue}}=0.83068+(0.11872\hat{\alpha})+(0.11555\widehat{SA})-(0.06195\widehat{GS}) -(0.03928\hat{\alpha}\,\widehat{SA})-(0.02635\hat{\alpha}\,\widehat{GS})-(0.01310\widehat{SA}\,\widehat{GS}) +(0.00431\hat{\alpha}\,\widehat{SA}\,\widehat{GS}) \tag{18}$$

Each normalized variable takes a value between -1 and $+1$, with zero representing the median value. A paradrogue for which the strut angle is 67.5 deg, gore spacing is 6.75 deg, and canopy characteristic length is 4.25 in. (all median values from that study) has a drag

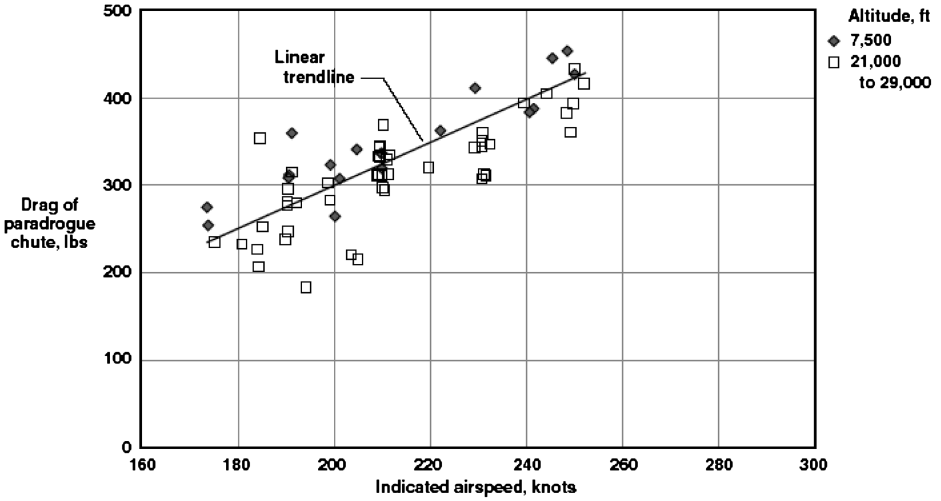

Fig. 5 Steady-state drag of paradrogue assembly from the flight-test data. (This figure is taken from [3] and used with permission of NASA.)

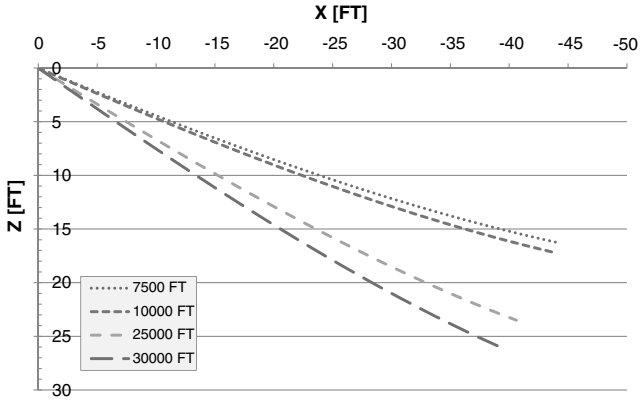

Fig. 6 Steady-state positions of the hose-paradrogue assembly (side view) ($V_\infty = 210$ kt).

coefficient of $C_{\text{drogue}} = 0.83068$. A nominal value of $C_{\text{drogue}} = 0.8$ was used in the numerical predictions of steady-state positions of the hose-paradrogue assembly presented in the sequel.

Recently, there are considerable demands on innovative technologies that actively stabilize and control the drogue motion in-flight, especially for UAV refueling purposes. In the development of such technologies, it is important to understand the dynamic characteristics of the hose-drogue assembly subject to actuation inputs. Reference [1] suggests that paradrogue drag is strongly dependent on strut angle. In this study, the dynamic motion of a hose-drogue assembly subject to in-flight changes of the paradrogue strut angle is investigated. The drag coefficient changes are estimated using a reduced form of Eq. (18). Using the median values for variables other than the strut angle,

$$C_{\text{drogue}} = 0.83068 + 0.11872\hat{\alpha} \tag{19}$$

Details of the physical mechanism required to control the strut angle are not presented.

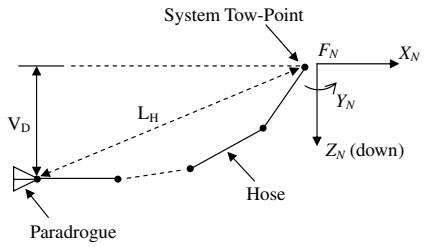

a)

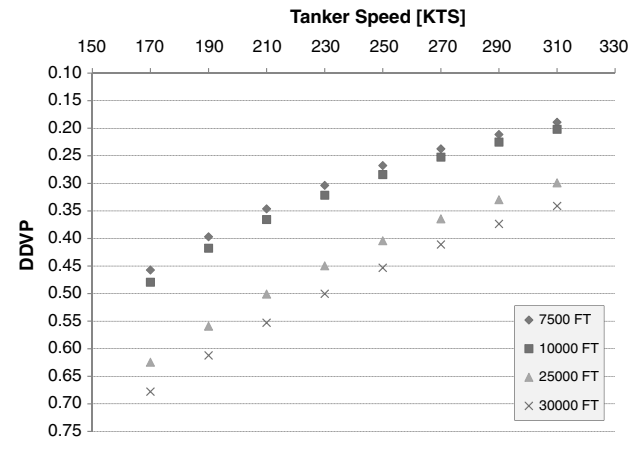

b)

Fig. 7 Plots of a) dimensionless drogue vertical position, DDVP = V_D/L_H and b) paradrogue dimensionless vertical position vs tanker speed.

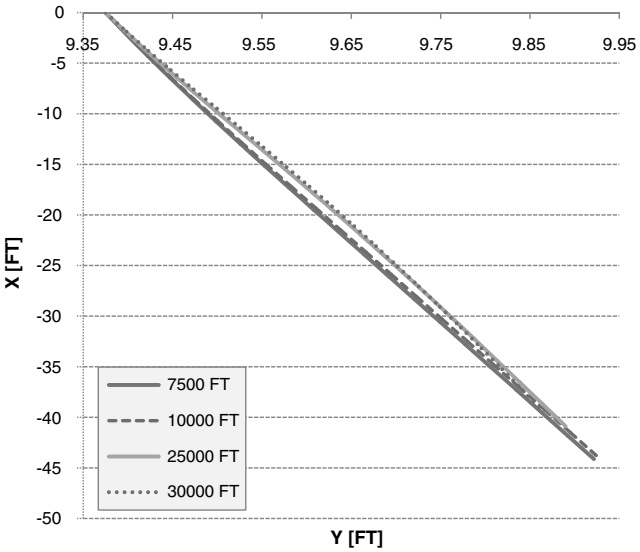

Fig. 8 Top view of out-of-plane, steady-state positions ($V_\infty = 210$ kt); refueling pod located at midspan of right wing.

III. Numerical Solution Procedure

Given the physical and geometrical data for the hose-drogue assembly and the tanker characteristics, the motion of the mean trajectory frame F_W, the motion of the system tow point relative to

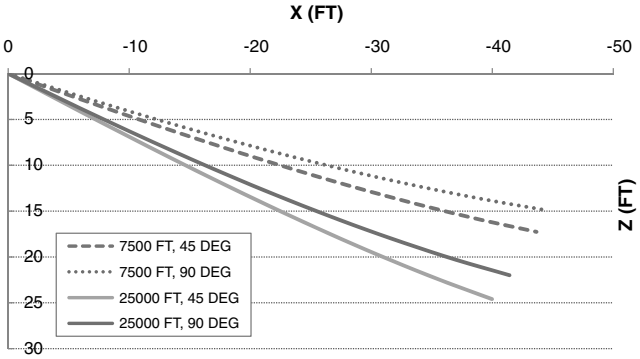

a)

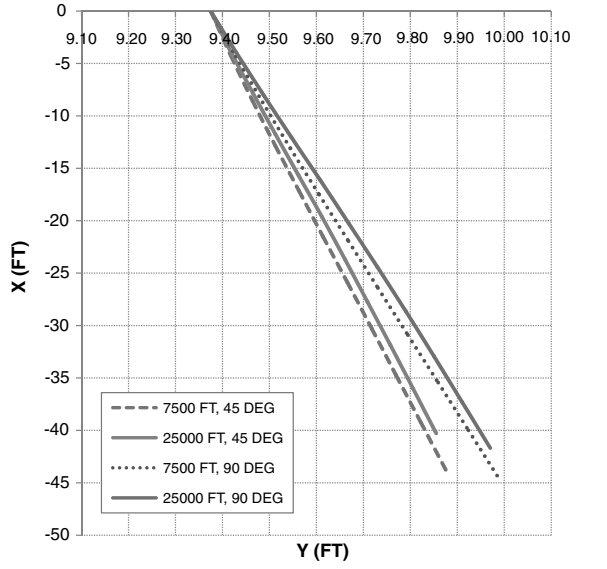

b)

Fig. 9 Plots of a) side view of steady-state positions ($V_\infty = 210$ kt) and b) top view of out-of-plane steady-state positions ($V_\infty = 210$ kt); refueling pod located at midspan of right wing.

F_W, and the initial conditions of all link angles, the following procedure may be used to track the motion of the system.

1) Compute the position and velocity vectors of the lumped masses.

2) Compute $\boldsymbol{Q}_K$ the external (weight and drag) force vectors for each lumped mass.

3) Formulate and solve the link tension Eq. (10). Exploit the sparseness of $[T]$.

4) Compute the lumped mass accelerations using Eq. (7).

5) Compute the second derivatives of the link angles using Eq. (6).

6) Numerically integrate to find a set of link angles and their derivatives at the next time.

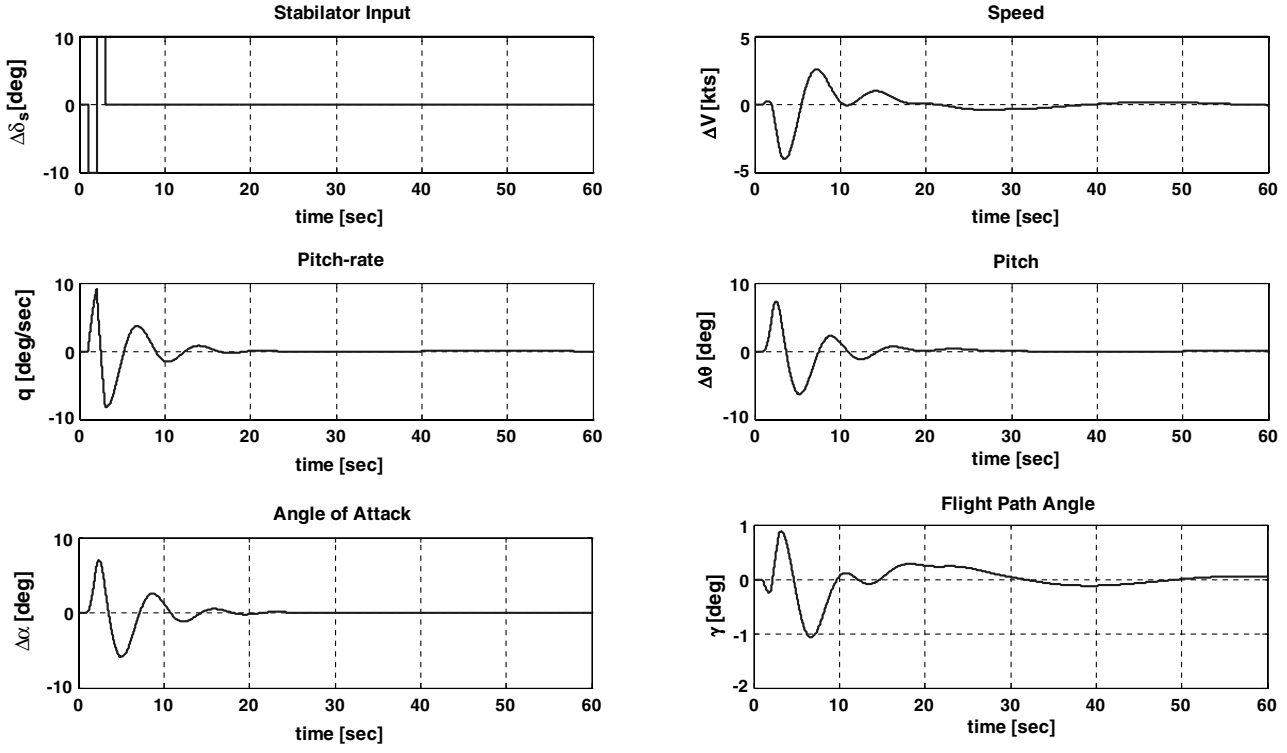

a)

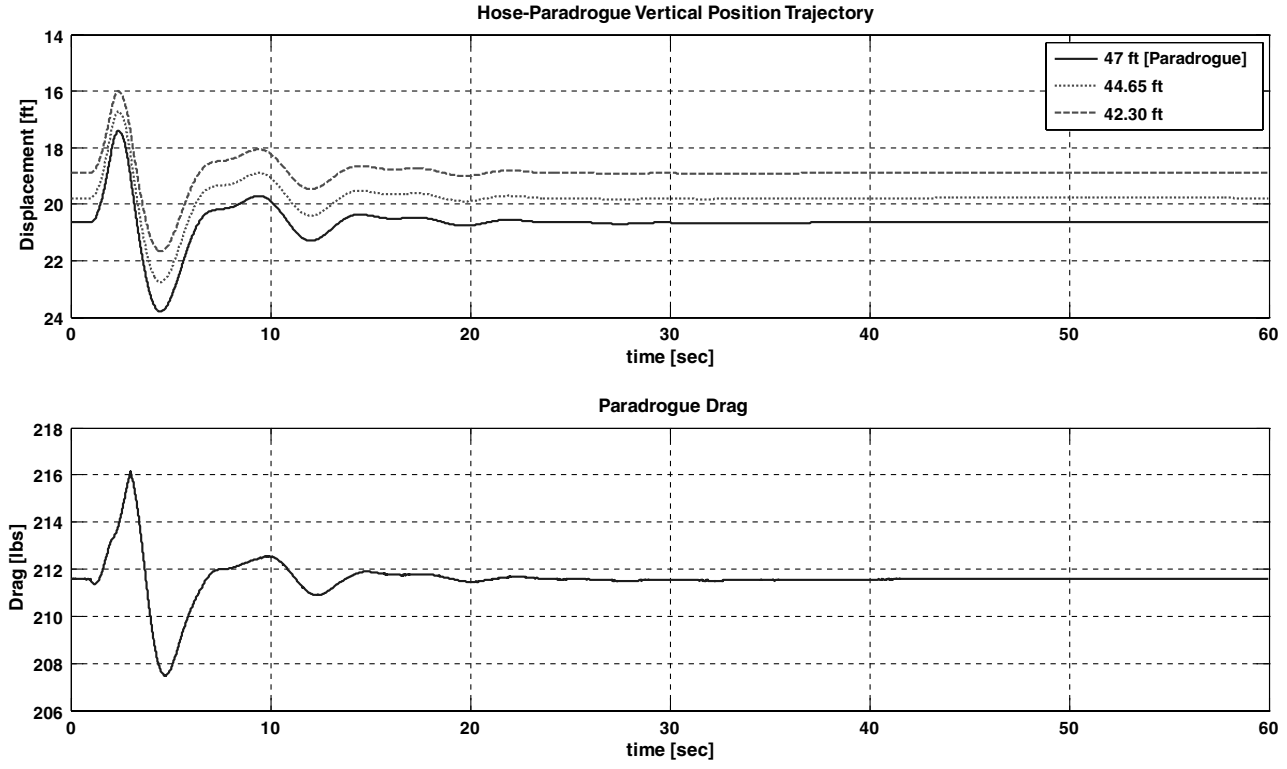

b)

Fig. 10 Plots of a) tanker pitch doublet maneuver ($V_\infty = 210$ kt and alt $= 7500$ ft) and b) hose-paradrogue-assembly response to tanker pitch doublet maneuver ($V_\infty = 210$ kt and alt $= 7500$ ft).

7) Repeat steps 1 through 6 to track the motion for future times.

Table 1 summarizes the physical characteristics of the hose-paradrogue assembly [12] and the tanker [2,3] used for numerical studies presented in the following section.

IV. Simulation Results

A MATLAB script simulation program was developed based on the mathematical model presented in the previous section. A fourth-order fixed-step Runge–Kutta method is used to numerically integrate the equations of motion with a 20-segment hose model. The following describes some of the simulation results. Comparisons are made whenever possible to published results from flight tests and numerical simulations.

A. Steady-State Characteristics

The steady-state position of the hose-paradrogue assembly for various flight conditions is of fundamental interest for safe aerial refueling. This position may be approximated by numerically solving the governing differential equations of motion until a steady-state solution is obtained. Table 2 shows the computed steady-state values of the hose-paradrogue assembly under typical refueling conditions. For all cases, the system reaches a steady-state configuration within 20 s. As previously mentioned, a nominal paradrogue drag coefficient of 0.8 is used for all cases, and the results are compared with published flight-test results [2,3].

1. Paradrogue Drag and Hose Tension

Figure 4 shows a graph of the computed steady-state paradrogue drag data from Table 2, which clearly shows the effects of speed and altitude. At an altitude of 7500 ft (2286 m), the computed drag ranges from approximately 212 lb (943 N) at 170 kt (287 ft/s or 87.5 m/s) to 435 lb (1935 N) at 250 kt (422 ft/s or 129 m/s). The flight-test data show drag values ranging from 200 to 450 lb (890 to 2002 N) over the same speed range [2,3]. Reference [3] states that paradrogue drag appears to vary linearly with speed over this same range. This effect is also evident from the computed results in Fig. 4.

Although the computed results clearly show the effect of altitude on drag (associated with changes in air density), [3] states there is no discernible effect of altitude on drag. This discrepancy may be due to the fact that the model computes air density using the properties of the standard atmosphere [16]. These computed densities may be different from those experienced during the flight tests. Careful observation of the published data in Fig. 5, however, suggests there is an altitude effect. Most of the drag values measured at higher altitudes of 21,000 to 29,000 ft (6400 to 8839 m) are below the values measured at 7500 ft (2286 m).

The maximum hose tension occurs at the hose exit point from a refueling pod. A maximum computed value of approximately 695 lb (3092 N) occurs at the highest airspeed (310 kt or 523 ft/s or 159 m/s) and the lowest altitude (7500 ft or 2286 m). This is well below the hose fracture tension reported to be greater than 3000 lb (13.34 kN) [12].

2. Paradrogue Position

Figure 6 shows steady-state positions of the hose-paradrogue assembly at various altitudes for a tanker speed of 210 kt (354 ft/s or 108 m/s). The paradrogue is observed to be in a higher position (relative to the tanker) at lower altitudes where the paradrogue drag is larger. References [2,3] introduce a dimensionless parameter, DDVP $= V_D/L_H$ (dimensionless drogue vertical position), to characterize the steady-state position of the paradrogue relative to the tanker. The distances V_D and L_H are illustrated in Fig. 7a. This parameter is computed from the simulation results and is presented in Table 2 and graphed in Fig. 7b. The trend of the computed results matches well with the flight-test results presented in [2]. The flight-test data show approximately 6.5 to 7 ft (1.98 to 2.13 m) differences in static drogue vertical positions at airspeeds ranging from 195 kt (329 ft/s or 100 m/s) to 295 kt (498 ft/s or 152 m/s) regardless of altitude. The simulation results show 8.7 to 11.2 ft (2.65 to 3.41 m) differences at airspeeds ranging from 190 kt (321 ft/s or 97.7 m/s)

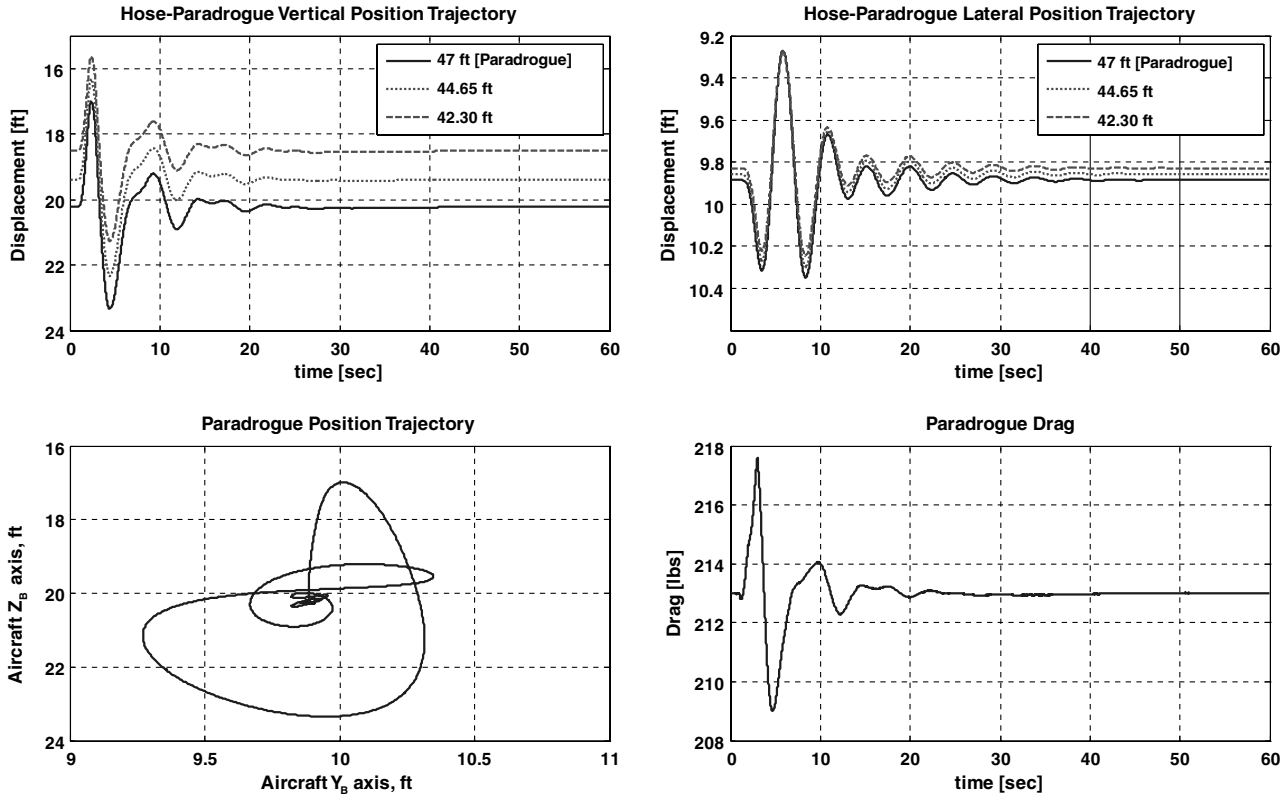

Fig. 11 Hose-paradrogue-assembly response to tanker pitch doublet maneuver ($V_\infty = 210$ kt and alt $= 7500$ ft); refueling pod located at midspan of right wing.

to 290 kt (489 ft/s or 149 m/s) with the larger differences occurring at higher altitudes.

If a refueling pod (and hence the hose exit position) is located off the tanker symmetry plane in the span wise direction of the wing, the hose-drogue assembly is subject to an asymmetric tanker wake. This results in steady side-wash on the assembly due to wingtip vortices. (See Fig. 3) The result is a small steady-state, out-of-plane displacement of less than 1 ft. Figure 8 illustrates steady-state positions of the assembly for a towing speed of 210 kt (354 ft/s or 108 m/s) when the refueling pod is located at midspan of the right wing.

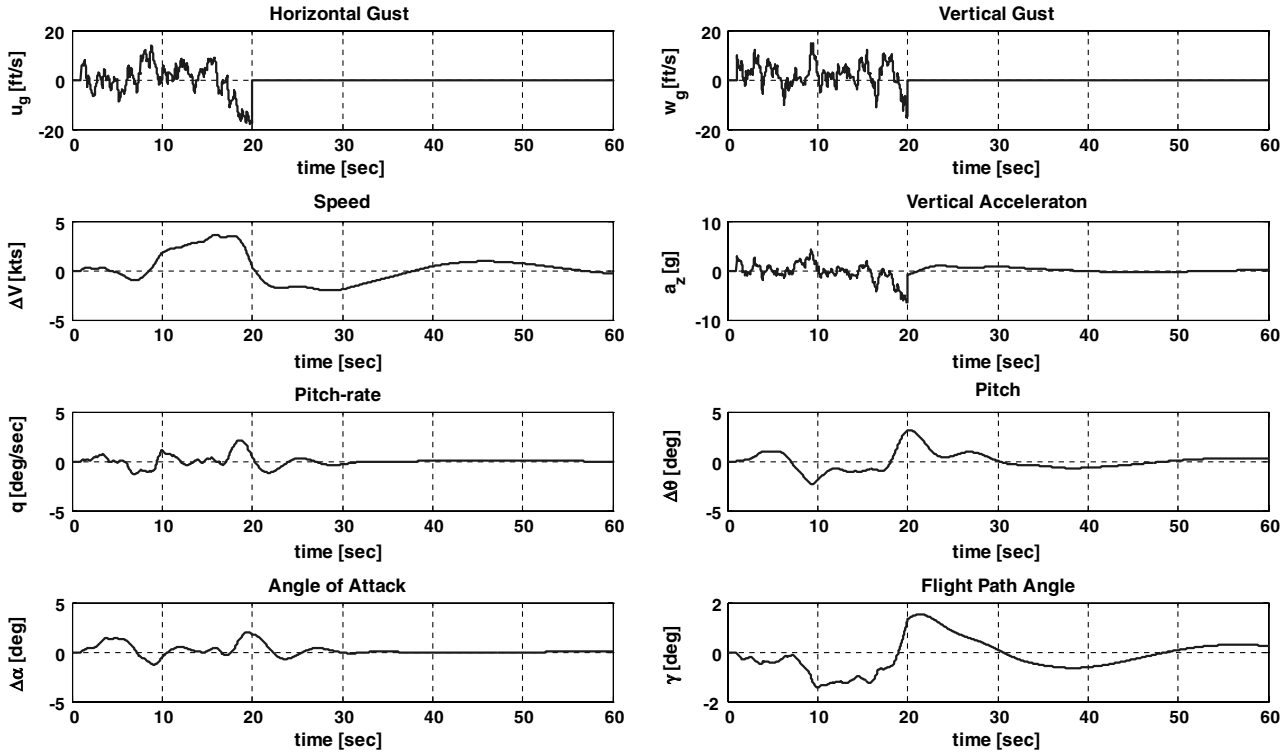

a)

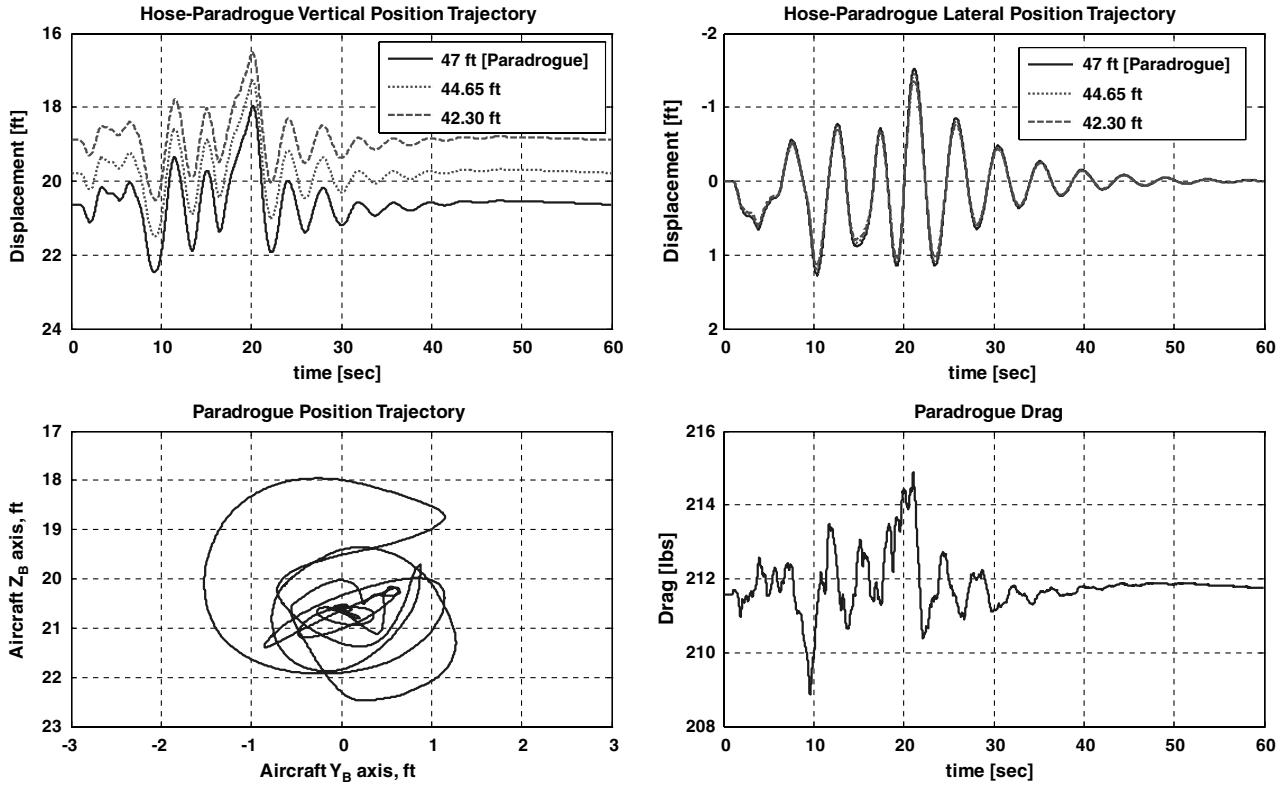

b)

Fig. 12 Plots of a) tanker motion subject to atmospheric turbulence ($V_\infty = 210$ kt and alt = 7500 ft) and b) hose-paradrogue-assembly response to atmospheric turbulence ($V_\infty = 210$ kt and alt = 7500 ft).

3. Variable-Drag Paradrogue

Reference [3] presented wind-tunnel test results for lower-drag and higher-drag paradrogue assemblies and states that the lower-drag paradrogue is highly desirable as it trails lower behind the tanker when deployed. Here, Eq. (19) is used to study a variable-drag paradrogue assembly based on changes of the drogue's strut angle. Steady-state positions for two drogue strut angles are shown in Fig. 9. The simulation results also clearly show that the lower-drag paradrogue model (strut angle of 45°) trails lower behind the tanker, as illustrated in Fig. 9a. If the refueling pod is located at midspan of the right wing, the higher-drag paradrogue has a somewhat larger out-of-plane displacement, as shown in Fig. 9b.

B. Dynamic Characteristics

Reference [2] identifies the effect of tanker maneuvering on the dynamics of the hose-paradrogue assembly as a research problem requiring further study. In this section, the dynamic response of the hose-drogue assembly is computed to a typical pitch doublet tanker maneuver initiated from a steady level cruise flight. Also studied are the dynamic responses associated with atmospheric turbulence and in-flight strut-angle changes. Strut-angle changes are considered as a means of stabilizing and steering the drogue's position relative to the tanker. All dynamic simulations were performed at 210 kt (354 ft/s or 108 m/s) and altitude of 7500 ft (2286 m).

1. Response to Tanker Pitch Maneuver

To understand the response of the hose-paradrogue assembly to realistic tanker motions, a typical pitch doublet maneuver response is simulated. A linear longitudinal dynamic model of an F-18 was constructed using stability derivatives found in [17] and was used to compute the tanker motion. Figure 10a shows the tanker response to a $\pm 10°$ stabilator doublet with 1 s duration, starting at $t = 1$ s. Figure 10b shows the resulting vertical displacement of three hose locations: the paradrogue node at 47 ft (14.3 m) and hose nodes at 44.65 ft (13.6 m) and 42.3 ft (12.9 m) as measured from the towing point. Figure 10b also shows how the paradrogue drag changes during the maneuver. The maximum vertical displacement of the paradrogue experienced during this maneuver is about 5.5 ft (1.68 m), which is close to the flight-test value of about 6.5 ft (1.98 m) (measured using a flight video system) [2].

As mentioned earlier, the hose-drogue assembly also experiences an out-of-plane or lateral oscillatory motion due to the tanker wake when the refueling pod is located at the midspan of one of the wings. Figure 11 shows the lateral motions of the assembly for the tanker pitch doublet maneuver with the refueling pod at midspan of the right wing. In this case, the system exhibits somewhat more oscillatory behavior, perhaps due to the asymmetric tanker wake.

2. Response to Atmospheric Turbulence

The flight-test study in [2] reports that the impact of turbulence on the dynamic characteristics of the hose-drogue system was significant. When the system encountered light turbulence on a calm day, the drogue did not stabilize which made it difficult to determine steady-state positions and to perform a refueling engagement. This situation is studied here by incorporating the Dryden wind-turbulence model [18] into the hose-paradrogue model. The results below are for light turbulence (turbulence intensity of 10^{-2}) with a length scale of 1750 ft (533 m). This length scale corresponds to an F-18 traveling at 210 kt (354 ft/s or 108 m/s) and altitude of 7500 ft (2286 m). All three velocity components were used in the simulation. Turbulence effects on the hose and paradrogue drag and the tanker motion were included. The tanker response was again computed using the F-18 linear dynamic model.

Figure 12a shows a 20 s duration of turbulent air velocity (starting at $t = 1$ (s)) and the subsequent tanker response. Figure 12b shows the resulting vertical and lateral displacement trajectories of the three locations on the hose-drogue assembly. Because of the presence of the lateral component of the atmospheric gust, the assembly also undergoes lateral motion even when the refueling pod is located in the plane of symmetry of the tanker. When the refueling pod is located at midspan of the right wing, the assembly undergoes a

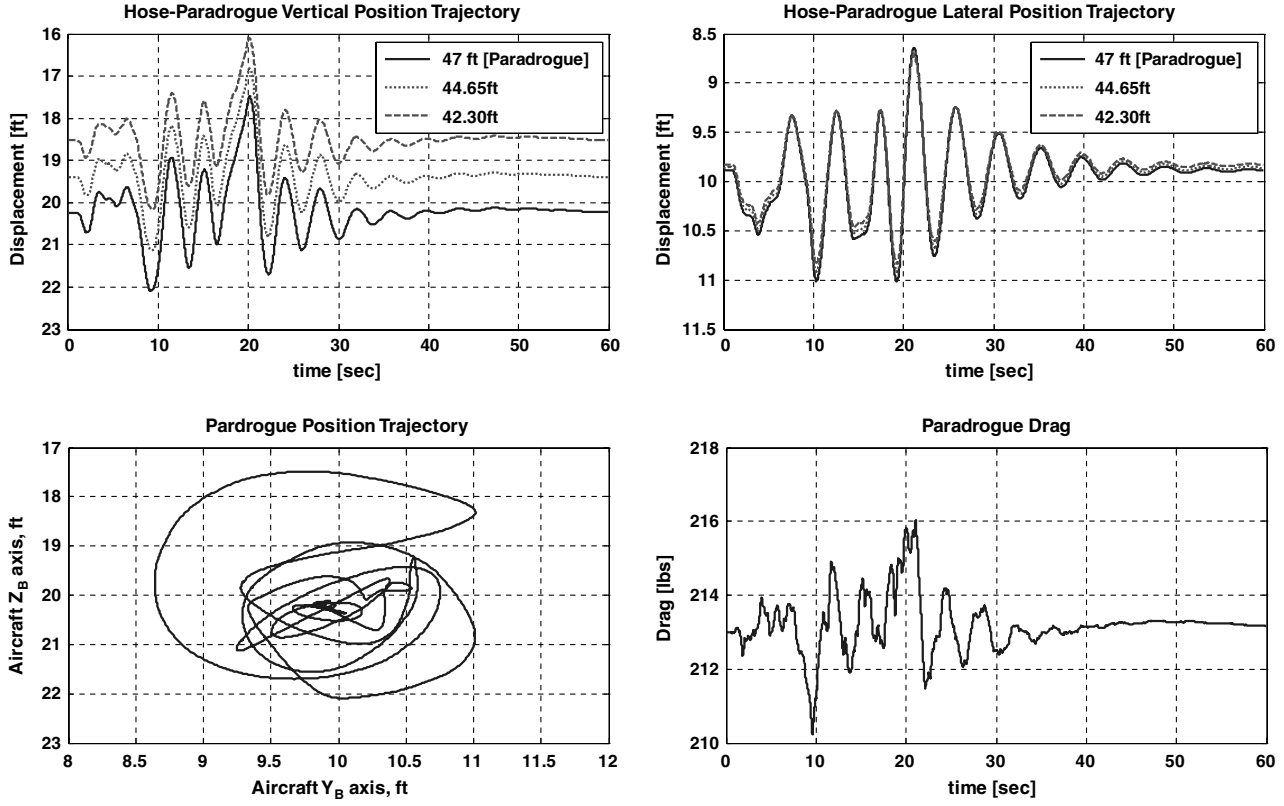

Fig. 13 Hose-paradrogue-assembly response to atmospheric turbulence ($V_\infty = 210$ kt and alt = 7500 ft); refueling pod located at midspan of right wing.

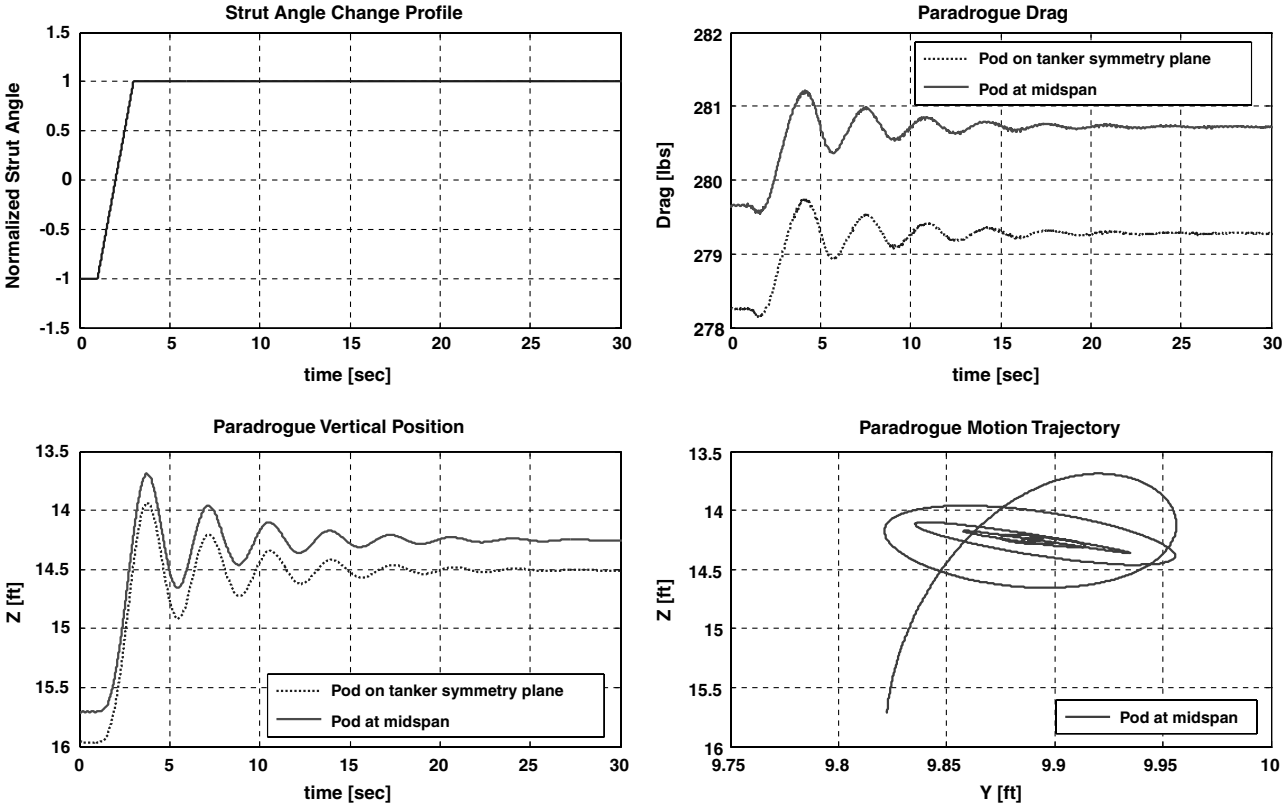

Fig. 14 Dynamic response of the paradrogue assembly to in-flight strut-angle change ($V_\infty = 210$ kt and alt = 7500 ft).

similar motion trajectory (Fig. 13), because the magnitude of the turbulent air velocity is substantially larger than the tanker wake-induced velocity. For both cases the paradrogue undergoes 4.0 to 4.5 ft (1.22 to 1.37 m) vertical and 2.5 to 3.0 ft (0.762 to 0.914 m) lateral displacements during the presence of turbulence, and it fails to settle into a steady-state position as described in the flight-test study.

3. Response to In-Flight Change of Paradrogue Drag Coefficient

As discussed earlier, some innovative methods to actively stabilize and control the motion of the paradrogue in flight are greatly needed. Here, a numerical simulation is presented to investigate the motion of the paradrogue assembly when the paradrogue's strut angle (and hence its drag) is changed in flight. Figure 14 shows the input strut-angle profile and the open-loop response of the hose-paradrogue assembly for refueling pods located on the tanker symmetry plane and at midspan of the right wing. The strut angle is changed from 45 to 90° (normalized strut angle from -1 to $+1$). Equation (19) is used to model the corresponding drag coefficient changes.

The system response to the ramp increase of strut angle is lightly damped. The drogue position oscillates vertically for about 5 cycles during the initial 20 s and stabilizes to a new steady-state value, resulting in 1.0 to 1.5 ft (0.305 to 0.457 m) vertical distance changes and 1 lb (4.45 N) paradrogue drag changes. The control authority for this paradrogue appears to be low; however, changes in its geometric characteristics may produce better results. Note that when the refueling pod is located at the midspan of the right wing, the system exhibits a similar initial out-of-plane oscillatory response as noted in earlier simulations.

C. Remarks on Numerical Accuracy

A fourth-order, fixed-step, Runge–Kutta method was used to numerically integrate the equations of motion for the hose-paradrogue model. To minimize numerical and modeling inaccuracies, convergence studies were performed at an airspeed of 210 kt (354 ft/s or 108 m/s) and altitude of 7500 ft (2286 m) for the number of hose links (N) and the fixed time step Δt. Models with 10, 20, 30, 40, 50, and 60 links and time steps of 10^{-4}, 5×10^{-4}, 10^{-3}, 5×10^{-3}, and 10^{-2} (s) were studied. In each case, the motion of the system was computed as it transitioned from an initial perturbed state to its final steady-state configuration. The vertical position of the paradrogue was used for comparison. The differences in the paradrogue positions in the models using 20, 30 and 40 segments were less than 6.08×10^{-4} ft (1.85×10^{-4} m), and the differences in the positions using time increments of 10^{-4}, 5×10^{-4}, 10^{-3}, 5×10^{-3}, and 10^{-2} (s) were less than 7.64×10^{-6} ft (2.33×10^{-6} m). Consequently, all of the above results were generated using 20 links and a fixed time step of $\Delta t = 0.01$ (s).

V. Conclusions

A dynamic model of a hose-paradrogue assembly for aerial refueling was developed using the finite-segment approach, and a MATLAB script program was developed for numerical simulation studies. Simulations of paradrogue drag and position relative to the tanker aircraft under steady-state refueling conditions compare favorably with previously reported flight-test results. Dynamic simulations of paradrogue vertical position changes in response to a tanker pitch doublet maneuver are also comparable.

The effects of atmospheric turbulence on paradrogue motion is studied by incorporating the Dryden turbulence model into the hose-paradrogue dynamic model. The simulation results show the paradrogue is unable to maintain a steady-state position relative to the tanker in the presence of turbulence. A similar result was reported by a NASA flight test in which the motion was found to make it difficult for the receiver aircraft to engage with the refueling system. The possibility of controlling the drogue position in flight by adjusting the drogue's strut angle is also investigated using a variable-drag paradrogue aerodynamic model.

The dynamic model developed herein may be readily altered to study the coupling procedure with a receiver aircraft. In this case, the paradrogue end of the hose also has specified motion as prescribed by the closure rate of the refueling aircraft. In addition, the link connected to the refueling store/pod can be modeled as a variable-length segment, thus allowing for the study of postcontact hose tension control using a motor-driven reel drum in the pod system.

The receiver forebody wake model can be also augmented to the present dynamic model, which may allow understanding of its impact on the hose-paradrogue assembly.

References

[1] Ro, K., Basaran, E., and Kamman, J. W., "Aerodynamic Characteristics of Paradrogue Assembly in an Aerial Refueling System," *Journal of Aircraft*, Vol. 44, No. 3, May–June 2007, pp. 963–970. doi:10.2514/1.26489

[2] Hensen, J. H., Murray, J. E., and Campos, N. V., "The NASA Dryden AAR Project: A Flight Test Approach to an Aerial Refueling System," AIAA Atmospheric Flight Mechanics Conference and Exhibit, AIAA Paper 2004-4939, Aug. 2004.

[3] Vachon, M. J., Ray, R. J., and Calianno, C., "Calculated Drag of an Aerial Refueling Assembly Through Airplane Performance Analysis," NASA TM-2004-212043, Feb. 2004.

[4] Bolkcom, C., "Air Force Aerial Refueling Methods: Flying Boom Versus Hose-and-Drogue," Congressional Research Service, The Library of Congress, Order Code RL32910, June 2006.

[5] Valasek, J., Gunnam, K., Kimmett, K., Tandale, M. D., and Junkins, J. L., "Vision-Based Sensor and Navigation System for Autonomous Air Refueling," *Journal of Guidance, Control, and Dynamics*, Vol. 28, No. 5, Sept.–Oct. 2005, pp. 979–989. doi:10.2514/1.11934

[6] Zhu, Z. H., and Meguid, S. A., "Elastodynamic Analysis of Aerial Refueling Hose Using Curved Beam Element," *AIAA Journal*, Vol. 44, No. 6, 2006, pp. 1317–1324. doi:10.2514/1.17311

[7] Kamman, J. W., and Nguyen, T. C., "Modeling Towed Cable System Dynamics," Naval Surface Warfare Center, Panama City Div., TM-492-88, Panama City, FL, May 1990.

[8] Kamman, J. W., and Huston, R. L., "Modeling of Variable Length Towed and Tethered Cable Systems," *Journal of Guidance, Control, and Dynamics*, Vol. 22, No. 4, 1999, pp. 602–608. doi:10.2514/2.4423

[9] Vassberg, J. C., Yeh, D. T., Blair, A., and Evert, J. M., "Dynamic Characteristics of a KC-10 Wing-Pod Refueling Hose by Numerical Simulation," 20th Applied Aerodynamics Conference, AIAA Paper 2002-2712, St. Louis, MO, June 2002.

[10] Vassberg, J. C., Yeh, D. T., Blair, A., and Evert, J. M., "Numerical Simulations of KC-10 Wing-Mount Aerial Refueling Hose-Drogue Dynamics with a Reel Take-Up System," 21st Applied Aerodynamics Conference, AIAA Paper 2003-3508, Orlando, FL, June 2003.

[11] Vassberg, J. C., Yeh, D. T., Blair, A., and Evert, J. M., "Numerical Simulation of KC-10 Centerline Aerial Refueling Hose-Drogue Dynamics with a Reel Take-Up System," 22nd Applied Aerodynamics Conference, AIAA Paper 2004-4719, Province, RI, June 2004.

[12] Vassberg, J. C., Yeh, D. T., Blair, A., and Evert, J. M., "Numerical Simulation of KC-10 In-Flight Refueling Hose-Drogue Dynamics with an Approaching F/A-18D Receiver Aircraft," 22nd Applied Aerodynamics Conference, AIAA Paper 2005-4605, Toronto, June 2005.

[13] Hoerner, S. F., *Fluid-Dynamic Drag*, published by the author, Midland Park, NJ, 1965, pp. 3-3, 3-12, 15-4, 16-13, 19-17.

[14] Schmidt, L. V., *Introduction to Aircraft Flight Dynamics*, AIAA Education Series, AIAA, Reston, VA, 1998, pp. 49–56.

[15] Dogan, A., Lewis, T. A., and Blake, W., "Flight Data Analysis and Simulation of Wind Effects During Aerial Refueling," *Journal of Aircraft*, Vol. 45, No. 6, 2008, pp. 2036–2048. doi:10.2514/1.36797

[16] Anderson, J. D., Jr., *Introduction to Flight*, 6th ed., McGraw–Hill, New York, 2007, pp. 105–124.

[17] Iliff, K. W., and Wang, C. K., "Flight-Determined Subsonic Longitudinal Stability and Control Derivatives of the F-18 High Angle of Attack Research Vehicle (HARV) with Thrust Vectoring," NASA TP-97-206539, Dec. 1997.

[18] "Flying Qualities of Piloted Airplanes," U.S. Dept. of Defense, MIL-SPEC MIL-F-8785C, Nov. 1980.